Transferable interactions of Li^{+} and Mg^{2+} ions in polarizable models

Vered Wineman-Fisher,[†] Julián Meléndez Delgado,[†] Péter R. Nagy,[‡] Eric Jakobsson,[¶] Sagar A. Pandit,[§] and Sameer Varma[*,†,§]

[†]*Department of Cell Biology, Microbiology and Molecular Biology, University of South Florida, Tampa, Florida, USA*

[‡]*Department of Physical Chemistry and Materials Science, Budapest University of Technology and Economics, H-1521 Budapest, P.O.Box 91, Hungary*

[¶]*National Center for Supercomputing Applications, Center for Biophysics and Computational Biology, Department of Molecular and Integrative Physiology, University of Illinois at Urbana-Champaign, Urbana, Illinois, USA*

[§]*Department of Physics, University of South Florida, Tampa, Florida, USA*

E-mail: svarma@usf.edu

Abstract

Therapeutic implications of Li^+, in many cases, stem from its ability to inhibit certain Mg^{2+}-dependent enzymes, where it interacts with or substitutes for Mg^{2+}. The underlying details of its action are, however, unknown. Molecular simulations can provide insight, but their reliability depends on how well they describe relative interactions of Li^+ and Mg^{2+} with water and other biochemical groups. Here we explore, benchmark and recommend improvements to two simulation approaches, one that employs an all-atom polarizable molecular mechanics (MM) model, and the other that uses a hybrid quantum and molecular mechanics implementation of the quasi-chemical theory (QCT). The strength of the former is that it describes thermal motions explicitly, and that of latter is that it derives local contributions from electron densities. Reference data is taken from experiment, and also obtained systematically from CCSD(T) theory, followed by benchmarked vdW-inclusive density functional theory. We find that the QCT model predicts relative hydration energies and structures in agreement with experiment, and without need for additional parameterization. This implies that accurate descriptions of local interactions are essential. Consistent with this observation, recalibration of local interactions in the MM model, which reduces errors from 10.0 to 1.4 kcal/mol, also fixes aqueous phase properties. Finally, we show that ion-ligand transferability errors in the MM model can be reduced significantly from 10.3 to 1.2 kcal/mol by correcting the ligand's polarization term, and introducing Lennard-Jones cross-terms. In general, this work sets up systematic approaches to evaluate and improve molecular models of ions binding to proteins.

Introduction

Li^+ is an essential nutrient, but at high concentrations, it is toxic.[1] At low-to-intermediate concentrations, Li^+ is also considered as a therapeutic agent. It is a generally accepted first line therapy for bipolar disorder,[2] and it is also useful as an augmentation to other antidepressants in treatment of unipolar depression.[3] Several lines of evidence also suggest that Li^+ may be a component of therapy or prevention against neurodegenerative disorders[4] and cancer.[5] Our analysis of the human "Li^+ interactome," which is a network of genes interacting with Li^+-sensitive genes, shows strong mutual enrichment with KEGG pathways associated with neurodegenerative diseases[6] and cancer.[7]

A primary mode by which Li^+ affects physiological function is the one in which it inhibits the activities of certain Mg^{2+}-dependent phosphoryl-transfer enzymes, including phosphatases, kinases, and adenylyl cyclases.[1,8,9] Based on structural and biochemical studies on phosphatases,[10–12] Li^+ is expected to bind to these enzymes by competing against Mg^{2+}, and substituting for it in the enzyme's catalytic core (competitive binding). Alternatively, NMR[13] and quantum chemical[14] studies show that in solution, free ATP loads Li^+ and Mg^{2+} simultaneously, leading to the proposition that Li^+ could also bind to the catalytic core without altering the numbers of bound Mg^{2+} (cooperative binding). Regardless of Li^+'s binding mode, the molecular mechanism of how Li^+ affects their activities remains unknown. In fact, in a screening of over seventy human kinases at elevated Li^+ concentrations, Bain et al.[15] reported that many were affected and to varying degrees, but there is no explanation for these variations.

Molecular simulations can, in principle, provide the necessary energetic basis to understand these competitive and cooperative binding effects of Li^+. This, however, requires accurate and computationally efficient descriptions of relative interactions of Li^+ and Mg^{2+} with water and other relevant organic groups. Here we explore and validate two simulation models, one that employs the all-atom polarizable AMOEBA molecular mechanics (MM) force field,[16] and the other that is based on a hybrid quantum and implicit solvent imple-

mentation of the quasi-chemical theory (QCT).[17,18] The advantage of the former method over the latter is that it explicitly describes thermal motions and long ranged electrostatics. The advantage of the latter approach is that it derives all local contributions from a broad range of molecular forces, including charge-redistribution, polarization and dispersion, directly from self-consistent electron densities, rather than through their classical interpretations in MM models. In addition, the quasi-chemical formulation inherently provides an understanding of solvation and binding in terms of contributions from ligand density and number, as well as local and long-ranged effects.

Toward this end, we first benchmark a vdW-inclusive quantum density functional theory (DFT) against experiment and high-level quantum mechanical calculations. We then use it to obtain reference data for gas-phase interactions of ions with water and two other biochemical groups, methanol and N-methyl acetamide, which are representative small molecules of the hydroxyl and carbonyl functional groups found in Mg-binding sites in proteins.[1] We use this reference data alongside experiments to recommend the necessary improvements to both the MM and QCT models in the gas and condensed phases.

Methods

Reference energies

Coupled cluster single double and perturbative triple excitation (CCSD(T)) theory is significantly more expensive than density functional theory (DFT), and so we restrict its application to obtain reference information to benchmark a vdW-inclusive DFT. Specifically, we employ CCSD(T) in combination with complete basis set (CBS) extrapolation[19,20] to compute Mg^{2+}-water binding energies. We employ Dunning's correlation-consistent basis sets augmented with diffuse functions (aug-cc-pVXZ, X=T, Q, 5) for first row elements, and the corresponding core-valence basis sets[21] for Mg^{2+}. Sub-valence electrons of Mg^{2+} are correlated in the CCSD(T) calculations, while deep-core electrons of all atoms are kept frozen.

The basis set incompleteness error (BSIE) of the CBS(Q,5) interaction energies are estimated as the difference of the CCSD(T) energies obtained with CBS(T,Q) and CBS(Q,5). The local natural orbital (LNO) scheme[22,23] is employed to accelerate the CCSD(T) calculations as implemented in the MRCC package.[24,25] Approximation-free CCSD(T) energy and corresponding local error estimates are evaluated using the Tight and very Tight LNO-CCSD(T) threshold sets[23,26] according to the extrapolation scheme of Ref. 26. The cumulative BSIE and local error estimates indicate that the LNO-CCSD(T)/CBS(Q,5) interaction energies are within ±0.4 kcal/mol of the approximation-free CCSD(T)/CBS ones for all studied complexes.

The DFT that we benchmark is PBE0+vdW.[27,28] The PBE0 hybrid functional contains 25% exact exchange and is supplemented by Tkatchenko-Scheffler self-consistent corrections for dispersion (vdW). All PBE0+vdW calculations are performed using the FHI-AIMS package[29] with 'really tight' basis sets. Total energies are converged to within 10^{-6} eV and electron densities are converged to within 10^{-5} electrons. Geometry optimizations are carried out with force criterion of 10^{-3} ev/Å and the PBE0+vdW functional. The ion-ligand cluster geometries used in CCSD(T) are those obtained from PBE0+vdW optimizations.

Molecular dynamics simulations

All MD simulations are performed using TINKER[16] version 7.1. Integration is carried using the RESPA integrator with an outer time step of 1 fs.[16] The Bussi thermostat[30] and Monte Carlo barostat[31,32] with a coupling constant of 0.1 ps are employed to control temperature (T=298 K) and pressure (P=1 bar), respectively. Electrostatics is treated using the PME approach with a direct space cutoff of 9 Å. The convergence cutoff for induced dipoles is set to 0.01 D and the van der Waals interactions are computed explicitly within a 9 Å radius.

Free energies

Condensed phase – Bennett's acceptance ratio

Hydration free energies of ions in explicit solvent are computed using Bennett's acceptance ratio (BAR).[30] The conformational ensembles needed for BAR are obtained from molecular dynamics. Bennett shows that an almost optimal solution to estimate the free energy difference (ΔG) between equally sampled states A and B is obtained by: (a) minimizing the variance of the FEP average, which is done by choosing the Fermi-Dirac distribution $f(x) = 1/(1+e^x)$ as weighting factor, and (b) offsetting the energy by a scalar c in such way that the error is minimized. c is determined from the following equation in a self-consistent manner to ensure $c \approx \Delta G$

$$e^{-\beta(\Delta G - c)} = \frac{\langle f(\beta(U_B - U_A - c))\rangle_A}{\langle f(\beta(U_A - U_B - c))\rangle_B} \tag{1}$$

In the equation above, $\beta = 1/k_bT$. U_a and U_b are the potential energies obtained for the same configuration but computed using functions describing respectively, states A and B. The triangular brackets represent averages over configurational space sampled in states, A or B, indicated by subscripts.

To obtain overlap between U_A and U_B, and thus reduce the variance in the estimation of ΔG,[30] we compute the solvation free energies in multiple steps.[33,34] We first scale down the charges and polarizabilities of ions. In systems containing Li^+, this is done in 10 steps with $\lambda = \{1, 0.9, ..., 0.1, 0\}$, and in systems containing Mg^{2+}, this in done in 20 steps with $\lambda = \{1, 0.95, ..., 0.05, 0\}$. Each step is simulated for 200 ps under NVT conditions, and the final 100 ps are used to calculate ΔG.

Each system consists of 1500 water molecules, and either a single cation or a salt molecule (LiCl or $MgCl_2$). For a given system, the starting configurations of all its λ-simulations are identical. They are taken from a trajectory equilibrated under NPT conditions for 500 ps. The final 200 ps of this trajectory is used for calculating average box lengths, and the

snapshot that has the closest box length to this average is used as the starting configuration for λ-simulations.

Following computation of ΔG using BAR, the correction term $-RT \ln C_l/C_g = 1.9$ kcal/mol is added to adjust for ion concentration differences between gas ($C_g = 0.041$ M) and condensed ($C_l = 1$ M) phases.[18]

Condensed phase – Implicit solvent model

Hydration free energies of ion-ligand clusters in implicit solvent are obtained from two solutions to the static Poisson model, one in a dielectric medium of $\epsilon = 1$, and the other in a dielectric medium of $\epsilon = 78.5$, that is, $\Delta G^{aq} = G(78.5) - G(1)$. Poisson's equations are set up numerically by describing atoms using the ParSE (Parameters for Solvation Energy) parameter set,[35] and defining dielectric boundaries using a solvent probe radius of 1.4 Å about the ParSE atomic radii. The region not occupied by solvent is assigned a dielectric $\epsilon = 2$, consistent with ParSE parameterization. The Poisson's equation is solved using a multigrid approach implemented in the `APBS v 1.3` package.[36] For all calculations, the finest grid spacing is set at 0.138 Å, and the spatial extent of the outer grid size is set at 100 Å. Reducing the outer grid size by half changes energies by less than 0.5 kcal/mol.

Gas phase – Harmonic approximation

The thermal component to the Gibbs free energy of a cluster in the gas phase is estimated using the ideal gas thermodynamic relationship, $G_{corr} = F_{corr} + 1/\beta$, where F_{corr} is the correction to the Helmholtz free energy. Assuming that the coupling between translational, vibrational and rotational degrees of freedom can be neglected, F_{corr} is estimated as a sum of their independent contributions,[37] that is, $F_{corr} = F_{trans} + F_{vib} + F_{rot}$, where

$$F_{trans} = -1/\beta \left[\ln \left(\frac{m}{2\pi\hbar^2\beta} \right)^{3/2} + \ln \frac{1}{\beta P} + 1 \right], \tag{2}$$

$$F_{vib} = E + \sum_{i}^{3N-6} \left[\frac{\hbar\omega_i}{2} + 1/\beta \ln\left(1 - \exp^{-\beta\hbar\omega_i}\right) \right], \quad (3)$$

and

$$F_{rot} = -\frac{3}{2\beta} \ln \left[\frac{2}{\beta\hbar^2} (I_A I_B I_C)^{1/3} \pi^{1/3} \right]. \quad (4)$$

In the expressions above, N is the number of atoms in the molecule, I_A, I_B, and I_C are the molecular moments of inertia, $P = 1$ atmosphere, m is the molecular mass and ω_i are the harmonic vibrational frequencies obtained from a Hessian analysis of the PBE0 energy surface. Wave functions are described using the 6-311++G** basis set, and we note that switching to a Dunning's correlation consistent basis set (aug-cc-pVDZ) increases ion-ligand binding free energies by an average of 0.7 kcal/mol. These calculations are performed using Gaussian09.[38]

Results

Ion-water interactions in the gas phase

Reference energies

We demonstrated previously that the PBE0 density functional[27] augmented with self-consistent dispersion corrections (PBE0+vdW)[28] yields interaction energies of Na^+ and K^+ ions with water, methanol and formamide molecules in excellent agreement with CCSD(T) and Quantum Monte Carlo (QMC).[34,39] We have also noted previously[40] that under a harmonic approximation, PBE0+vdW predicts gas phase ion-water cluster enthalpies and free energies consistent with experiment. Therefore, we continue to use PBE0+vdW to obtain reference data for interactions of Li^+ ions with water, methanol and N-methylacetamide (NMA) molecules.

Table 1 compares predictions of Mg^{2+}-water binding energies from PBE0+vdW against

LNO-CCSD(T). Ion-water binding energies are defined as

$$\Delta E = E_{\mathrm{AW_n}} - n \times E_{\mathrm{W}} - E_{\mathrm{A}}, \tag{5}$$

where, $E_{\mathrm{AW_n}}$, E_{W} and E_{A} are, respectively, the electronic energies of ion-water clusters, isolated water molecule and isolated ions following independent energy optimizations. n is the number of water molecules in the ion-water cluster. With a mean absolute error (MAE) < 0.5 kcal/mol, the correspondence is excellent. Based on our earlier work,[39] and the error measures corresponding to the LNO approximations being below 0.15 kcal/mol, we expect that the LNO scheme[22,23] employed to accelerate CCSD(T) retains its intrinsic accuracy.

Table 1: Comparison of Mg^{2+}-water binding energies computed using LNO-CCSD(T) and PBE0+vdW. Binding energies are normalized by the number of water molecules in clusters, and are in units of kcal/mol.

n	LNO-CCSD(T)	PBE0+vdW
1	-82.4	-83.6
2	-77.8	-78.6
3	-71.6	-72.1
4	-65.8	-65.9
5	-59.2	-59.2
6	-54.4	-54.3

Table 2 compares experimental gas phase ion-water binding free energies against those obtained from PBE0+vdW. The gas phase ion-water binding free energies are computed by adding harmonic and analytical thermal corrections Gibb's energy (see methods) to ΔE obtained from Equ. 5. Note that the 5- and 6-fold clusters of Li^+ as well as the 7- and 8-fold clusters of Mg^{2+} used in computing free energies do not contain all waters in their respective first coordination shells (see Figure S1 of Supporting Information). This is because their binding energies were less favorable compared to those in which a subset of waters were outside their inner shells, just as we noted previously for Na^+ and K^+ ions.[18] For ion-water clusters in which all waters are interacting directly, the computed values are on average overestimated by 1.2 kcal/mol. For the 7- and 8-fold Mg^{2+}-water clusters in which one

and two waters are, respectively, in the ion's second shell, the binding free energies are off by a similar magnitude, but generally underestimated. Given that the computed ΔE in Table 1 agree well with LNO-CCSD(T), it appears that the discrepancies in free energies result from the harmonic approximation employed in computing the vibrational contributions to free energies. Nevertheless, the errors introduced by harmonic approximations are still small enough to keep the computed free energies close to the desired chemical accuracy of 1 kcal/mol.

Table 2: Comparison of experimental gas phase free energies against those obtained from PBE0+vdW with harmonic and analytical thermal components to Gibb's energy. All energies are in kcal/mol.

	n	Expt.	PBE0+vdW
Li^+	1	-25.5	-28.0
	2	-18.9	-21.8
	3	-13.3	-13.0
	4	-7.5	-7.5
	5	-4.5	-2.1
	6	-2.5	-2.6
Mg^{2+}	6	-16.0	-17.0
	7	-12.8	-10.9
	8	-10.9	-9.6

Recalibration of ionic descriptors in MM model

Table 3 shows that the ion-water binding energies predicted from the original AMOEBA model[41,42] are substantially off with respect to our reference values. Additionally, the error is systematic – the predicted values are underestimated, and the extent of underestimation also grows with cluster size. For the 6-fold Li^+ clusters, the error reaches 7 kcal/mol, and for the Mg^{2+} cluster, the error gets larger than 20 kcal/mol.

We, therefore, re-calibrate the descriptors of Li^+ and Mg^{2+} ions against our new reference data and include as part of the target set all of the PBE0+vdW data listed in Table 3. In

the AMOEBA model, vdW interactions are described using a buffered 14-7 function,

$$U_{vdw} = \epsilon_{ij} \left(\frac{1.07}{\rho_{ij} + 0.07} \right)^7 \left(\frac{1.12}{\rho_{ij}^7 + 0.12} - 2 \right), \tag{6}$$

where ϵ_{ij} in kcal/mol is the potential well depth, and $\rho_{ij} = r_{ij}/r_{ij}^0$, where r_{ij} in Ångströms is the distance between sites i and j and r_{ij}^0 is the minimum energy distance. Re-optimizing the vdW descriptors of Li^+ against the new target data reduces the MAE in binding energies from 7.4 to 2.3 kcal/mol, but slightly decreases Li^+-oxygen distance. The ion-water cluster geometries energy optimized using the recalibrated model, however, remain similar to those obtained from PBE0+vdW (Figure S1 of the Supporting Information). The recalibrated descriptors of Li^+ (ϵ, r^0), which we refer to as the Pol* model, are (0.059, 1.906), while the original vdW descriptors were (0.08, 2.38).

In the case of Mg^{2+}, we also recalibrate a dimensionless parameter in its polarization term, as done in the development of the original and improved descriptors.[42–44] AMEOBA employs a Thole approach[45] to prevent polarization catastrophe, wherein electrostatic interactions are damped in the short range. Damping is applied to only one of the two sites of an interaction pair using $\rho = \frac{3a}{4\pi} e^{-a r_{ij}^3/\sqrt{\alpha_i \alpha_j}}$, where r_{ij} is the distance between two sites with atomic polarizabilities α, and 'a' is a dimensionless width parameter of the damped charge distribution that controls the damping strength. The parameter a is typically assigned a value of 0.39 to reproduce molecular polarizabilities and cluster energies of water and other molecules.[45–49] The data in Table 3 shows that recalibration of ϵ, r^0, and a results in significant improvement in Mg^{2+}-water binding energies. The mean error in binding energy reduces from 15.0 to 0.6 kcal/mol, but just as in the case of Li^+, the Mg^{2+}-oxygen distances decrease slightly (Table 3) with minimal affect on cluster geometry (Figure S1 of the Supporting Information). The recalibrated descriptors of Mg^{2+} (ϵ, r^0, a), which we also refer to as the Pol* model, are (0.45, 2.05, 0.085), while the the original descriptors were (0.3, 2.94,0.0952).

Table 3: Ion-water binding energies (ΔE in kcal/mol) and optimum distances (d in Å) prior to (Orig[41,42] and Orig*[43,44]) and after recalibration (Pol*) of ion descriptors against PBE0+vdW. The ion-water binding energy is defined using Equ. 5, and d is the distance between the ion and the oxygen atom of water. MAE is an abbreviation for mean absolute error.

Ion	# waters	PBE0+vdW		Orig		Orig*		Pol*	
		ΔE	d	ΔE	d	ΔE	d	ΔE	d
Li^+	1	-36.0	1.82	-33.2	1.82			-36.9	1.72
	2	-66.9	1.85	-61.1	1.88			-66.9	1.78
	3	-90.6	1.89	-81.9	1.94			-88.3	1.86
	4	-107.7	1.95	-97.7	2.01			-104.1	1.93
	5	-116.6	2.06	-107.2	2.07			-112.5	1.99
	6	-125.7	2.13	-117.8	2.15			-122.6	2.10
Mg^{2+}	1	-83.6	1.91	-78.0	1.88	-83.3		-83.6	1.84
	2	-157.1	1.93	-146.4	1.91	-155.0		-157.1	1.87
	3	-216.2	1.96	-201.2	1.96	-211.1		-215.7	1.91
	4	-263.7	1.99	-245.5	2.00	-255.7		-263.0	1.95
	5	-295.8	2.05	-276.1	2.04	-285.1		-294.8	1.99
	6	-325.5	2.09	-304.4	2.11	-312.8		-324.4	2.05
			MAE	10.0	0.02	6.5		1.4	0.05

Ion-water interactions in aqueous phase

Explicit solvent polarizable MM model

To evaluate the effect of MM model recalibration on aqueous phase properties, we first use BAR[30] to compute ion hydration free energies. However, instead of comparing hydration free energies of individual cations to experiment, we focus on comparing their relative hydration free energies. This is because experimental estimates of the former quantity depend on extra-thermodynamic assumptions that yield a wide spread in their estimates. In contrast, estimates of the relative hydration free energies are free from such assumptions.[50] As such, Li^+/Mg^{2+} competitive binding to proteins requires accurate estimates of the latter quantity. The extra-thermodynamic assumptions are essentially needed to separate out the energetics of salt dissolution into their constituent cationic and anionic contributions.[51,52] Two assumptions are commonly used, TATB and CPA. TATB assumes that the magnitudes of the solvation energies of tetraphenylarsonium (TA) and tetraphenylborate (TB) are equal.[51,53,54]

CPA refers to the cluster-pair approximation[55] in which the energetics of cations and anions in their individual solvent clusters are expected to converge toward each other rapidly following a monotonous trend, although recent studies suggest a more complex convergence.[56] These two assumptions, for example, produce Li^+ hydration free energies that differ by 10 kcal/mol (Table 4).

We carry out free energy calculations in two different ways. In one set, we simulate a single cation in a periodic box of 1500 waters and subject it to perturbation in BAR calculations. In the second set, we simulate a salt (LiCl or $MgCl_2$) in a periodic box of 1500 waters, and subject all ions in the box (2 in the case of LiCl and 3 in the case of $MgCl_2$) to simultaneous perturbations in BAR calculations so that the net charge of the periodic box remains neutral and constant in all λ-simulations.[57]

The results of these free energy calculations are provided in Table 4. For each case we report three different hydration free energy estimates, corresponding to different adjustments to air-water interface potentials ψ. Values denoted by ψ_0 are obtained directly from BAR calculations in bulk water, and so they do not include interface potential effects. This value may be compared directly to experimental values obtained using the TATB scheme, as this scheme is not expected to include air-water interface potential effects.[58,59] We note, however, that there is no consensus on either the magnitude or the sign of air-water interface potential.[60–64] Nevertheless, for the sake of comparison, we provide hydration free energy estimates in Table 4 that are adjusted for two different interface potentials, $\psi = -0.4$ V[63] and $\psi = +0.1$ V.[61,64] Adjustments are made as $\Delta G_\psi = eF\psi + \Delta G_{\psi=0}$, where '$e$' is the charge of the ion in electron units and 'F' is Faraday's constant.

When we simulate a single cation in a periodic box, we find that recalibration does improve $Li^+ \rightarrow Mg^{2+}$ free energy differences, however, an error of 5-6 kcal/mol remains with respect to experiment. This error, however, vanishes when we simulate and grow neutral salts, and compute $2Li^+ \rightarrow Mg^{2+}$ free energy differences. The error in the calculation of $Li^+ \rightarrow Mg^{2+}$ free energies can, therefore, at least partly be attributed to integrating charges in a

Table 4: Hydration free energies (in kcal/mol) of ions from experiments, QCT QM/MM model and all-atom MM models. Error estimates for single ion hydration energies in the MM model, which are obtained using Monte Carlo bootstrapping,[41] are all ≤ 0.1 kcal/mol. ψ_0 refers to hydration free energies lacking air-water interface potential effects. $\psi_{-0.4}$ and $\psi_{+0.1}$ refer to hydration free energies adjusted for two different surface potentials, $\psi = -0.4$ V[63] and $\psi = -0.1$ V,[61,64] respectively. Note that experimental TATB estimates are not expected to include interface potential effects, and, therefore, can be compared to ψ_0 values.[58,63] Experimental CPA estimates contain interface potential effects and so should be compared to $\psi_{-0.4}$ and $\psi_{+0.1}$. [a]Ref. 54 , [b]Ref. 53, [c]Ref. 55

	Polarizable MM						**QCT QM/MM**			**Experiment**		
	Orig			Pol*						TATB[a]	TATB[b]	CPA[c]
	ψ_0	$\psi_{-0.4}$	$\psi_{+0.1}$	ψ_0	$\psi_{-0.4}$	$\psi_{+0.1}$	ψ_0	$\psi_{-0.4}$	$\psi_{+0.1}$			
Li^+	-105.5	-114.7	-103.2	-111.9	-121.1	-110.6	-116.9	-126.1	-114.6	-116.9	-113.5	-126.5
Mg^{2+}	-408.7	-427.1	-404.1	-428.8	-446.2	-424.2	-443.3	-461.7	-438.7	-439.1	-437.4	
$Li^+ \rightarrow Mg^{2+}$	-303.2	-312.4	-300.9	-316.9	-326.1	-314.6	-326.4	-335.6	-324.1	-322.2	-323.9	
$2LiCl \rightarrow MgCl_2$	-200.9	-200.9	-200.9	-206.4	-206.4	-206.4	-209.5	-209.5	-209.5	-205.3	-210.4	

finite periodic boundary system, as demonstrated previously.[57] Note that the $2Li^+ \rightarrow Mg^{2+}$ free energy difference is insensitive to the assumption of the interface potential.

To examine the structure of water around ions, we compute the radial distributions of water oxygens around ions. We compute these from the final 4.5 ns of 5 ns long MD trajectories of single cations in water generated under isobaric and isothermal conditions. The results are shown in Figure 1. We note first that recalibration makes the inner shell of both ions tighter, consistent with enhanced stability of ion-water interactions in the recalibrated model. The positions of the first peak also change, but remain within the experimental ranger of $1.90 - 1.95$ Å for Li^+ and $2.00 - 2.12$ Å for Mg^{2+}.[65] The coordination number, that is, the number of waters within the first minima, remain unchanged at 6.0 for Mg^{2+} and decrease from 4.2 to 4.0 for Li^+. The coordination numbers from the recalibrated model match those from experiment and *ab inito* molecular dynamics simulations.[65,66]

Overall, we find that recalibrating ion-water interactions substantially improves their relative ion hydration free energies, but have a little effect on local structure, which as such was in agreement with experiment.

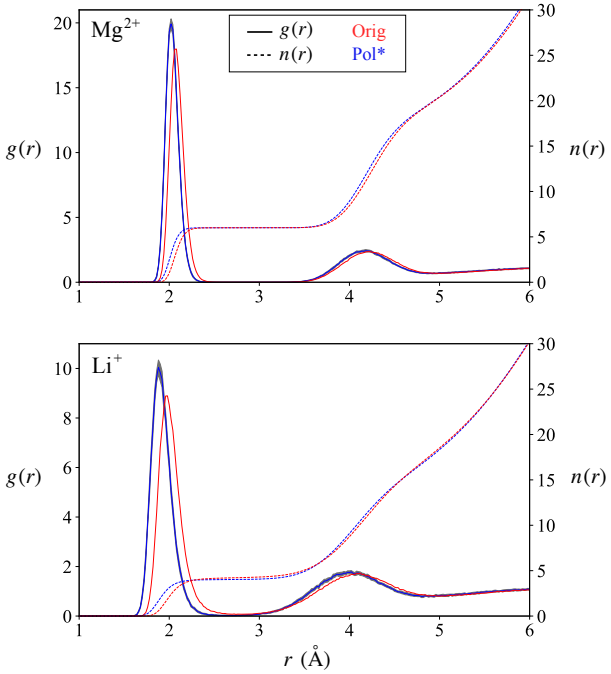

Figure 1: Radial distribution functions $g(r)$ and running integrations $n(r)$ of the water oxygens around ions determined from all-atom MM models. The standard deviation represented as a grey shade on the Pol* model is computed from block averaging.

QCT QM/MM model

The potential distribution theorem[17,67] defines the excess chemical potential or the hydration Gibbs free energy of a solute as $\Delta G = -1/\beta \ln\langle e^{-\beta\Delta U}\rangle$, where ΔU is the interaction energy of the solute with the surrounding waters. Introducing a conditional probability that the solute interacts with n waters (W) within an arbitrarily defined sub-volume Γ around the ion, leads to the relationship[17,18,50]

$$\Delta G = -1/\beta \ln\left[\sum_{n\geq 0} K_n^0 \left[\frac{\langle e^{-\beta\Delta U_{\mathrm{AW_n}}}\rangle_\Gamma}{[\langle e^{-\beta\Delta U_{\mathrm{W}}}\rangle]^n}\right](C_{\mathrm{W}})^n\right] \tag{7}$$

Here, K_n^0 is the "ideal" equilibrium constant of the association reaction $\mathrm{A}+n\mathrm{W} \rightleftharpoons \mathrm{AW}_n$, as it does not include any effects of the complementary region Γ^C outside the inner-shell domain. The specific effects of Γ^C are incorporated through the ensemble averages. At the same time K_n^0 is also not the gas-phase equilibrium constant because it is obtained under the condition

that the association equilibrium occurs within a predefined sub-volume, whereas the gas phase equilibrium constant is free from such an imposition. $\langle e^{-\beta\Delta U_{\mathrm{AW_n}}}\rangle_\Gamma$ is the ensemble average of the distribution that is the product of the distributions for the water molecules in Γ^C and for the complex enclosed within the region Γ. $\langle e^{-\beta\Delta U_{\mathrm{W}}}\rangle$ is essentially the excess chemical potential of a water molecule. Finally, C_{aq} is the concentration of water molecules in the aqueous phase.

In accord with the quasi-chemical formulation in Equ. 7, we calculate the hydration free energy of an ion, $\Delta G = \min\{\Delta G_n\}$ by summing up four terms[18]

$$\Delta G_n = \Delta G_{\mathrm{AW_n}} + \Delta G^{aq}_{\mathrm{AW_n}} - n\Delta G^{aq}_{\mathrm{W}} + \Delta G_{\mathrm{conc}}. \tag{8}$$

We compute $\Delta G_{\mathrm{AW_n}} = -1/\beta \ln K^0_n$ from quantum DFT so that all local interactions of ions with water are treated at the electronic level. $\Delta G^{aq}_{\mathrm{AW_n}}$ and the hydration free energy of a water molecule, $\Delta G^{aq}_{\mathrm{W}}$, are computed from solutions to Poisson's equation. The sub-volume Γ needed for these calculations is taken as a sphere around the ion with a radius equal to the first minimum in the RDF of water oxygens around the ion in the aqueous phase. We use the RDFs from the MD simulations reported above. Finally, $\Delta G_{\mathrm{conc}} = -1/\beta \ln(C_{aq}/C_g)$, where the aqueous and gas phase concentrations of water are taken as $C_{aq} = 55.6$ M and $C_g = 0.041$ M.

The results of these calculations are provided in Figure 2. For Li^+, the preferred coordination number is $n = 4$ that yields the smallest ΔG_n and a hydration free energy $\Delta G = -116.9$ kcal/mol. Similarly for Mg^{2+}, the preferred coordination number is 6 and $\Delta G = -443.3$ kcal/mol. The predicted preferred coordination numbers as well as relative hydration free energies of these ions match experimental estimates.[53,54,66] Absolute and relative free energies are provided in Table 4, and also adjusted for surface potentials in the same manner as described in the previous subsection. Note that the 7- and 8-fold Mg-water clusters reported in Table 2 are not used in these calculations because not all waters in these

clusters are within the pre-defined sub-volumes (Fig S1 of Supporting Information). Note also that the 5- and 6-fold Li-water clusters used in Table 2 are not the same as ones used here – the clusters used here have all waters in lithium's pre-defined sub-volume (Fig S1 of Supporting Information).

We also observed from Figure 2 that for both ions, the overall shapes of their ΔG_n profiles closely resemble their respective local cluster energies $\Delta G_{\mathrm{AW_n}}$ profiles, suggesting that the hydration properties of the these ions are dictated primarily by how they interact with waters in their inner coordination shells. Additionally, the local interactions $\Delta G_{\mathrm{AW_n}}$ contribute to more than half of the hydration free energy, and for both ions, this contribution is about 60%. These are precisely the reasons why getting local interactions, including many-body effects, is critical for predicting hydration free energies. This is also perhaps why a recalibration of local interactions of ions with water in the MM model (previous section) leads to significant improvements and reproduction of experimental hydration free energies.

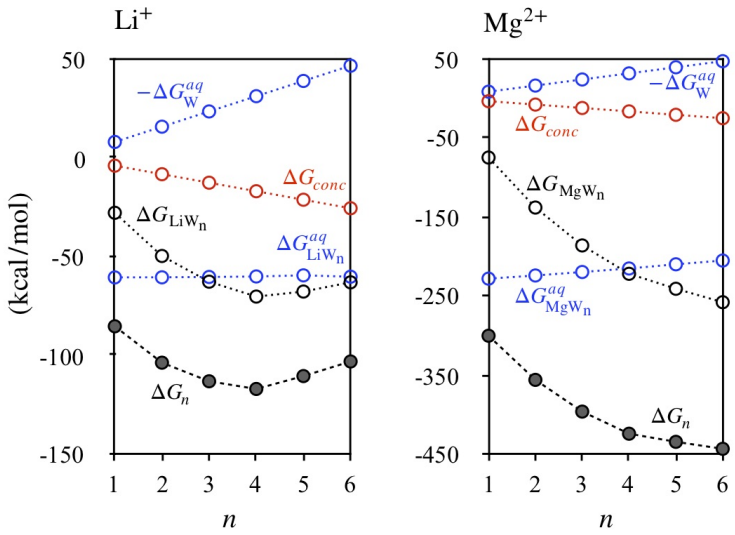

Figure 2: Quasi-chemical components in the calculation of the hydration free energies of Li^+ and Mg^{2+} ions.

Transferability of ionic interactions

Improving interactions of ions with water in the MM model does not, by itself, guarantee meaningful predictions of interactions of ions with other biochemical groups. To evaluate such transferability, we consider the substitution reaction below

$$\mathrm{AW}_n + n\mathrm{X} \rightleftharpoons \mathrm{AX}_n + n\mathrm{W}, \tag{9}$$

and determine the associated substitution energy as

$$\Delta E_{sub} = E_{\mathrm{AX}_n} - nE_{\mathrm{X}} - E_{\mathrm{AW}_n} + nE_{\mathrm{W}}. \tag{10}$$

Here 'A' refers to either a Li^+ or Mg^{2+} ion, 'W' refers to water and 'X' refers to a Methanol or NMA, which are molecules representative of two different chemical groups, hydroxyls and carbonyls, that are found in cation binding sites in proteins.

Figure 3 shows that the original MM model performs poorly in comparison to our reference data. The MAE for Li^+ is 3.9 kcal/mol and that of Mg^{2+} is much higher at 13.2 kcal/mol. Improving interactions of these ions with water, as we did above, will not improve their interactions with methanol and NMA, as we demonstrated recently in the case of other monovalent cations.[34]

One approach to improve transferability in MM models is to define cross-terms or separate sets of non-bonded (NB) descriptors for every distinct pair of ion and its coordinating chemical group (ligand).[44,68–74] In most applications,[68–74] the error corrections in this NBFix approach are assigned to the Lennard-Jones (LJ) term; however, there is no supporting information of this term being the source of error.

An alternative approach is to determine the error source and fix the underlying physics. We demonstrated recently[34] that one such error source for transferability in the AMEOBA model is its polarization term. Specifically, we noted that the contribution of polarization

to a ligand's binding energy was erroneous at the kind of high electric fields present near monovalent cations, although the model performs well in low dipolar electric fields where all MM models are calibrated and benchmarked. We have also shown recently[39] that when the polarization descriptors of ligands are themselves calibrated to satisfy reference data at high fields, their interactions also improve with ions, and without compromising performance at low fields. Methanol and NMA were among the two ligands we recalibrated as part of this effort.

Figure 3 reports the performance of these recalibrated models (Pol*) in predicting transferability. We find that the use of these model does reduce the Li^+ MAE to 1.9 kcal/mol, but that of Mg^{2+}, despite improvement, does stay quite large at 9.3 kcal/mol. Presumably, some physics essential to describing interactions of divalent cations is still misrepresented or missing in the MM model. This is supported by the observation that the residual errors in the recalibrated model are systematic, as in the binding energies of Mg^{2+} to both methanol and NMA are underestimated. Nevertheless, as we show in Figure 3, these errors can be eliminated by the NB-fix approach, where we generate separate sets of LJ cross-terms for each ion-ligand pair (table S1 of the supporting information), instead of computing them from Lorentz-Berthelot type LJ combination rules. After applying the NB-fix approach, transferability MAE reduces to 0.6 and 1.1 kcal/mol, respectively, for Li^+ and Mg^{2+} ions.

Conclusions

This work serves as a key step in the development of molecular simulations models needed to enable future investigations of relative binding effects of Li^+ and Mg^{2+} to proteins. We report CCSD(T) reference energies for Mg^{2+}-water clusters and find that the vdW-corrected PBE0 density functional reproduces them. We also show that the vdW-corrected PBE0 density functional also reproduces experimental gas phase ion-water binding free energies of Li^+ and Mg^{2+} ions. These results are consistent with our previous benchmarks on interactions of Na^+

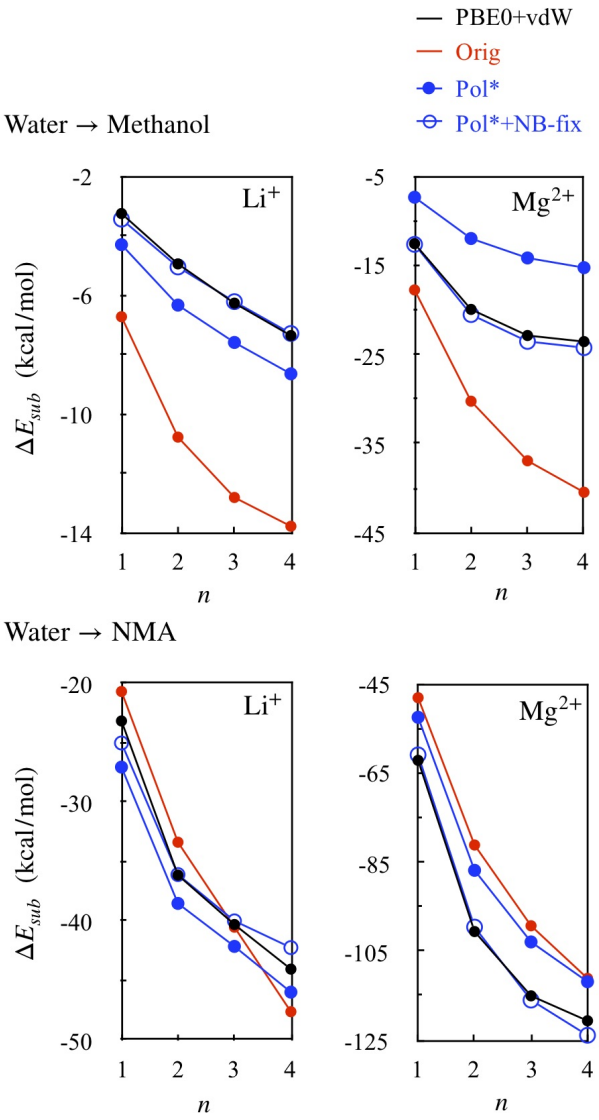

Figure 3: Water→Methanol and Water→NMA substitution energies (ΔE_{sub}) obtained before and after recalibration. Pol* refers to our recalibrated model of ligands[39] corrected for their dipolar field response, and Pol*+NB-fix refers to the model in which the remaining error in the Pol* model is corrected for by ignoring Lorentz-Berthelot type ion-ligand LJ combination rules, and introducing specific ion-ligand cross-terms.

and K^+ ions with various small molecules.[34,39,40] Using this reference data, we evaluate two molecular simulation models, one that employs an all-atom polarizable molecular mechanics (MM) force field, and the other that is based on a hybrid quantum and implicit solvent implementation of the quasi-chemical theory. Recalibration of the polarizable MM model substantially improves interactions of Li^+ and Mg^{2+} with water, with the mean absolute error reducing from 10.0 to 1.4 kcal/mol. Re-parameterization of local ion-water interactions also improves and yields relative hydration free energies of these ions in agreement with experiment. The QCT QM/MM model, which describes all ion-water local interactions at the QM level, also reproduces the experimental relative hydration free energies of these ions, and without any additional parameterization. The QCT analysis of energetic components also reveals that local interactions contribute substantially to hydration free energies, which provides rationale for why improvements in local interactions in the MM model lead to subsequent improvements in its prediction of hydration free energies. As expected though,[34] improvements in ion-water interactions do not automatically improve interactions of ions with other small molecules. Nevertheless, we show that transferability errors in the MM model can be reduced substantially from 10.3 to 1.2 kcal/mol by correcting the field response of the MM model's polarization term, and explicitly defining Lennard-Jones cross-terms for each ion-ligand pair. The need for introducing Lennard-Jones cross terms, especially for Mg^{2+} ions, suggests that there is still important underlying physics to be explored for doubly-charged cations.

In general, this work sets up approaches needed to both evaluate and improve molecular models of ions binding to proteins. The reference data generated here can also be used to evaluate and improve other MM models models, which can then be employed to study the binding of Li^+ and Mg^{2+} ions to biomolecules with greater reliability. Finally, we expect that the Li^+ study alone will also benefit lithium-battery technology, and the study of other lithium-based materials.[75]

Supplementary Material

Contains one table and one figure.

Acknowledgements

Authors acknowledge the use of computer time from Research Computing at USF, and the DECI resource Saga with support from the PRACE aisbl. We acknowledge funding from NIH grant number R01GM118697. PRN is grateful for financial support of NKFIH, Grant No. KKP126451, ÚNKP-19-4-BME-418 New National Excellence Program of the Ministry for Innovation and Technology and the János Bolyai Research Scholarship of the Hungarian Academy of Sciences.

Availability of Data

The data that support the findings of this study are available from the corresponding author upon reasonable request.

References

(1) Jakobsson, E.; Argüello-Miranda, O.; Chiu, S.-W.; Fazal, Z.; Kruczek, J.; Nunez-Corrales, S.; Pandit, S.; Pritchet, L. Towards a Unified Understanding of Lithium Action in Basic Biology and its Significance for Applied Biology. *The Journal of Membrane Biology* **2017**, *250*, 587–604.

(2) Grunze, H.; Vieta, E.; Goodwin, G. M.; Bowden, C.; Licht, R. W.; Azorin, J.-M.; Yatham, L.; Mosolov, S.; Möller, H.-J.; Kasper, S.; on behalf of the Members of the WFSBP Task Force on Bipolar Affective Disorders Working on this topic, The World Federation of Societies of Biological Psychiatry (WFSBP) Guidelines for the Biological Treatment of Bipolar Disorders: Acute and long-term treatment of mixed states in

bipolar disorder. *The World Journal of Biological Psychiatry* **2018**, *19*, 2–58, PMID: 29098925.

(3) Crossley, N. A.; Bauer, M. Acceleration and augmentation of antidepressants with lithium for depressive disorders: two meta-analyses of randomized, placebo-controlled trials. *J Clin Psychiatry* **2007**, *68*, 935–940.

(4) Forlenza, O. V.; De-Paula, V. J. R.; Diniz, B. S. O. Neuroprotective Effects of Lithium: Implications for the Treatment of Alzheimer's Disease and Related Neurodegenerative Disorders. *ACS Chemical Neuroscience* **2014**, *5*, 443–450, PMID: 24766396.

(5) Mazor, M.; Kawano, Y.; Zhu, H.; Waxman, J.; Kypta, R. M. Inhibition of glycogen synthase kinase-3 represses androgen receptor activity and prostate cancer cell growth. *Oncogene* **2004**, *23*, 7882–7892.

(6) Ge, W.; Jakobsson, E. Systems Biology Understanding of the Effects of Lithium on Affective and Neurodegenerative Disorders. *Frontiers in neuroscience* **2018**, *12*, 933–933.

(7) Ge, W.; Jakobsson, E. Systems Biology Understanding of the Effects of Lithium on Cancer. *Frontiers in oncology* **2019**, *9*, 296–296.

(8) Birch, N. J. Lithium and magnesium-dependent enzymes. *The Lancet* **1974**, *304*, 965–966.

(9) Phiel, C. J.; Klein, P. S. Molecular Targets of Lithium Action. *Annual Review of Pharmacology and Toxicology* **2001**, *41*, 789–813, PMID: 11264477.

(10) Li, Z.; Stieglitz, K. A.; Shrout, A. L.; Wei, Y.; Weis, R. M.; Stec, B.; Roberts, M. F. Mobile loop mutations in an archaeal inositol monophosphatase: Modulating three-metal ion assisted catalysis and lithium inhibition. *Protein Science* **2010**, *19*, 309–318.

(11) Haimovich, A.; Eliav, U.; Goldbourt, A. Determination of the Lithium Binding Site in Inositol Monophosphatase, the Putative Target for Lithium Therapy, by Magic-Angle-Spinning Solid-State NMR. *Journal of the American Chemical Society* **2012**, *134*, 5647–5651, PMID: 22384802.

(12) Dutta, A.; Bhattacharyya, S.; Dutta, D.; Das, A. K. Structural elucidation of the binding site and mode of inhibition of Li+ and Mg2+ in inositol monophosphatase. *The FEBS Journal* **2014**, *281*, 5309–5324.

(13) Briggs, K. T.; Giulian, G. G.; Li, G.; Kao, J. P. Y.; Marino, J. P. A Molecular Model for Lithiumś Bioactive Form. *Biophysical Journal* **2016**, *111*, 294–300.

(14) Dudev, T.; Grauffel, C.; Lim, C. How Native and Alien Metal Cations Bind ATP: Implications for Lithium as a Therapeutic Agent. *Scientific Reports* **2017**, *7*, 42377.

(15) Bain, J.; Plater, L.; Elliott, M.; Shpiro, N.; Hastie, C.; Mclauchlan, H.; Klevernic, I.; Arthur, J.; Alessi, D.; Cohen, P. The selectivity of protein kinase inhibitors: a further update. *Biochemical Journal* **2007**, *408*, 297–315.

(16) Shi, Y.; Xia, Z.; Zhang, J.; Best, R.; Wu, C.; Ponder, J. W.; Ren, P. Polarizable atomic multipole-based AMOEBA force field for proteins. *Journal of chemical theory and computation* **2013**, *9*, 4046–4063.

(17) Beck, T. L.; Paulaitis, M. E.; Pratt, L. R. *The Potential Distribution Theorem and Models of Molecular Solutions*; Cambridge University Press, 2006.

(18) Varma, S.; Rempe, S. B. Structural Transitions in Ion Coordination Driven by Changes in Competition for Ligand Binding. *Journal of the American Chemical Society* **2008**, *130*, 15405–15419.

(19) Karton, A.; Martin, J. M. L. Comment on: "Estimating the Hartree–Fock limit from finite basis set calculations". *Theor. Chem. Acc.* **2006**, *115*, 330.

(20) Helgaker, T.; Klopper, W.; Koch, H.; Noga, J. Basis-set convergence of correlated calculations on water. *J. Chem. Phys.* **1997**, *106*, 9639.

(21) Prascher, B. P.; Woon, D. E.; Peterson, K. A.; Dunning, T. H.; Wilson, A. K. Gaussian basis sets for use in correlated molecular calculations. VII. Valence, core-valence, and scalar relativistic basis sets for Li, Be, Na, and Mg. *Theor. Chem. Acc.* **2011**, *128*, 69.

(22) Nagy, P. R.; Kállay, M. Optimization of the linear-scaling local natural orbital CCSD(T) method: Redundancy-free triples correction using Laplace transform. *J. Chem. Phys.* **2017**, *146*, 214106.

(23) Nagy, P. R.; Samu, G.; Kállay, M. Optimization of the linear-scaling local natural orbital CCSD(T) method: Improved algorithm and benchmark applications. *J. Chem. Theory Comput.* **2018**, *14*, 4193.

(24) Kállay, M. et al. The MRCC program system: Accurate quantum chemistry from water to proteins. *J. Chem. Phys.* **2020**, *152*, submitted.

(25) MRCC, a quantum chemical program suite written by M. Kállay, P. R. Nagy, Z. Rolik, D. Mester, G. Samu, J. Csontos, J. Csóka, P. B. Szabó, L. Gyevi-Nagy, I. Ladjánszki, L. Szegedy, B. Ladóczki, K. Petrov, M. Farkas, P. D. Mezei, and B. Hégely. See http://www.mrcc.hu/ (Accessed October 1, 2019).

(26) Nagy, P. R.; Kállay, M. Approaching the basis set limit of CCSD(T) energies for large molecules with local natural orbital coupled-cluster methods. *J. Chem. Theory Comput.* **2019**, *15*, 5275.

(27) Adamo, C.; Barone, V. Toward reliable density functional methods without adjustable parameters: The PBE0 model. *The Journal of chemical physics* **1999**, *110*, 6158–6170.

(28) Tkatchenko, A.; Scheffler, M. Accurate Molecular Van Der Waals Interactions from

Ground-State Electron Density and Free-Atom Reference Data. *Physical Review Letters* **2009**, *102*, 073005(1)–073005(4).

(29) Blum, V.; Gehrke, R.; Hanke, F.; Havu, P.; Havu, V.; Ren, X.; Reuter, K.; Scheffler, M. Ab initio molecular simulations with numeric atom-centered orbitals. *Computer Physics Communications* **2009**, *180*, 2175–2196.

(30) Bennett, C. H. Efficient estimation of free energy differences from Monte Carlo data. *Journal of Computational Physics* **1976**, *22*, 245–268.

(31) Åqvist, J.; Wennerström, P.; Nervall, M.; Bjelic, S.; Brandsdal, B. O. Molecular dynamics simulations of water and biomolecules with a Monte Carlo constant pressure algorithm. *Chemical physics letters* **2004**, *384*, 288–294.

(32) Chow, K.-H.; Ferguson, D. M. Isothermal-isobaric molecular dynamics simulations with Monte Carlo volume sampling. *Computer physics communications* **1995**, *91*, 283–289.

(33) Grossfield, A.; Ren, P.; Ponder, J. W. Ion solvation thermodynamics from simulation with a polarizable force field. *Journal of the American Chemical Society* **2003**, *125*, 15671–15682.

(34) Wineman-Fisher, V.; Al-Hamdani, Y.; Addou, I.; Tkatchenko, A.; Varma, S. Ion-Hydroxyl Interactions: From High-Level Quantum Benchmarks to Transferable Polarizable Force Fields. *Journal of Chemical Theory and Computation* **2019**, *15*, 2444–2453, PMID: 30830778.

(35) Sitkoff, D.; Sharp, K. A.; Honig, B. Accurate Calculation of Hydration Free Energies Using Macroscopic Solvent Models. *The Journal of Physical Chemistry* **1994**, *98*, 1978–1988.

(36) Baker, N. A.; Sept, D.; Joseph, S.; Holst, M. J.; McCammon, J. A. Electrostatics

of nanosystems: Application to microtubules and the ribosome. *Proceedings of the National Academy of Sciences* **2001**, *98*, 10037–10041.

(37) McQuarrie, D. A. *Statistical Mechanics*; University Science Books, 2000.

(38) Frisch, M.; et. Al, Gaussian09 Revision A.1. **2009**,

(39) Wineman-Fisher, V.; Al-Hamdani, Y.; Nagy, P.; Tkatchenko, A.; Varma, S. Improved description of ligand polarization enhances transferability of ionic interactions. *Journal of Chemical Physics, Under revision*

(40) Rossi, M.; Tkatchenko, A.; Rempe, S. B.; Varma, S. Role of methyl-induced polarization in ion binding. *Proceedings of the National Academy of Sciences of the USA* **2013**, *110*, 12978–12983.

(41) Grossfield, A.; Ren, P.; Ponder, J. W. Ion Solvation Thermodynamics from Simulation with a Polarizable Force Field. *Journal of the American Chemical Society* **2003**, *125*, 15671–15682.

(42) Piquemal, J.-P.; Perera, L.; Cisneros, G. A.; Ren, P.; Pedersen, L. G.; Darden, T. A. Towards accurate solvation dynamics of divalent cations in water using the polarizable amoeba force field: From energetics to structure. *The Journal of Chemical Physics* **2006**, *125*, 054511.

(43) Liu, C.; Qi, R.; Wang, Q.; Piquemal, J.-P.; Ren, P. Capturing Many-Body Interactions with Classical Dipole Induction Models. *Journal of Chemical Theory and Computation* **2017**, *13*, 2751–2761, PMID: 28482664.

(44) Jing, Z.; Qi, R.; Liu, C.; Ren, P. Study of interactions between metal ions and protein model compounds by energy decomposition analyses and the AMOEBA force field. *The Journal of Chemical Physics* **2017**, *147*, 161733.

(45) Thole, B. T. Molecular polarizabilities calculated with a modified dipole interaction. *Chemical Physics* **1981**, *59*, 341–350.

(46) Ren, P.; Ponder, J. W. Polarizable atomic multipole water model for molecular mechanics simulation. *The Journal of Physical Chemistry B* **2003**, *107*, 5933–5947.

(47) Ren, P.; Ponder, J. W. Temperature and pressure dependence of the AMOEBA water model. *The Journal of Physical Chemistry B* **2004**, *108*, 13427–13437.

(48) Ren, P.; Wu, C.; Ponder, J. W. Polarizable Atomic Multipole-Based Molecular Mechanics for Organic Molecules. *Journal of Chemical Theory and Computation* **2011**, *7*, 3143–3161.

(49) Shi, Y.; Xia, Z.; Zhang, J.; Best, R.; Wu, C.; Ponder, J. W.; Ren, P. Polarizable Atomic Multipole-Based AMOEBA Force Field for Proteins. *Journal of Chemical Theory and Computation* **2013**, *9*, 4046–4063.

(50) Asthagiri, D.; Dixit, P.; Merchant, S.; Paulaitis, M.; Pratt, L.; Rempe, S.; Varma, S. Ion selectivity from local configurations of ligands in solutions and ion channels. *Chemical Physics Letters* **2010**, *485*, 1 – 7.

(51) Marcus, Y. Single ion Gibbs free energies of transfer from water to organic and mixed solvents. *Reviews in Analytical Chemistry* **1980**, *5*, 53–137.

(52) Pliego, J. R.; Miguel, E. L. M. Absolute Single-Ion Solvation Free Energy Scale in Methanol Determined by the Lithium Cluster-Continuum Approach. *The Journal of Physical Chemistry B* **2013**, *117*, 5129–5135, PMID: 23570440.

(53) Marcus, Y. The thermodynamics of solvation of ions. Part 4.—Application of the tetraphenylarsonium tetraphenylborate (TATB) extrathermodynamic assumption to the hydration of ions and to properties of hydrated ions. *Journal of the Chemical So-*

ciety, Faraday Transactions 1: Physical Chemistry in Condensed Phases **1987**, *83*, 2985–2992.

(54) Marcus, Y. *Ions in Solution and their Solvation*; John Wiley & Sons, 2015.

(55) Tissandier, M. D.; Cowen, K. A.; Feng, W. Y.; Gundlach, E.; Cohen, M. H.; Earhart, A. D.; Coe, J. V.; Tuttle, T. R. The Proton's Absolute Aqueous Enthalpy and Gibbs Free Energy of Solvation from Cluster-Ion Solvation Data. *102*, 7787–7794.

(56) Vlcek, L.; Chialvo, A. A.; Simonson, J. M. Correspondence between Cluster-Ion and Bulk Solution Thermodynamic Properties: On the Validity of the Cluster-Pair-Based Approximation. *The Journal of Physical Chemistry A* **2013**, *117*, 11328–11338, PMID: 24093538.

(57) Kastenholz, M. A.; Hünenberger, P. H. Computation of methodology-independent ionic solvation free energies from molecular simulations. II. The hydration free energy of the sodium cation. *The Journal of Chemical Physics* **2006**, *124*, 224501.

(58) Pliego, J. R.; Miguel, E. L. M. Absolute Single-Ion Solvation Free Energy Scale in Methanol Determined by the Lithium Cluster-Continuum Approach. *The Journal of Physical Chemistry B* **2013**, *117*, 5129–5135, PMID: 23570440.

(59) Pollard, T. P.; Beck, T. L. Re-examining the tetraphenyl-arsonium/tetraphenyl-borate (TATB) hypothesis for single-ion solvation free energies. *The Journal of Chemical Physics* **2018**, *148*, 222830.

(60) Pratt, L. R. Contact potentials of solution interfaces: phase equilibrium and interfacial electric fields. *The Journal of Physical Chemistry* **1992**, *96*, 25–33.

(61) Fawcett, W. R. The ionic work function and its role in estimating absolute electrode potentials. *Langmuir* **2008**, *24*, 9868–9875.

(62) Remsing, R. C.; Baer, M. D.; Schenter, G. K.; Mundy, C. J.; Weeks, J. D. The Role of Broken Symmetry in Solvation of a Spherical Cavity in Classical and Quantum Water Models. *The Journal of Physical Chemistry Letters* **2014**, *5*, 2767–2774, PMID: 26278076.

(63) Pollard, T. P.; Beck, T. L. The thermodynamics of proton hydration and the electrochemical surface potential of water. *The Journal of Chemical Physics* **2014**, *141*, 18C512.

(64) Duignan, T. T.; Baer, M. D.; Schenter, G. K.; Mundy, C. J. Electrostatic solvation free energies of charged hard spheres using molecular dynamics with density functional theory interactions. *The Journal of Chemical Physics* **2017**, *147*, 161716.

(65) Ohtaki, H.; Radnai, T. Structure and dynamics of hydrated ions. *Chemical Reviews* **1993**, *93*, 1157–1204.

(66) Varma, S.; Rempe, S. B. Coordination numbers of alkali metal ions in aqueous solutions. *Biophysical Chemistry* **2006**, *124*, 192–199, Ion Hydration Special Issue.

(67) Widom, B. Potential-distribution theory and the statistical mechanics of fluids. *The Journal of Physical Chemistry* **1982**, *86*, 869–872.

(68) Baker, C. M.; Lopes, P. E. M.; Zhu, X.; Roux, B.; MacKerell, A. D. Accurate Calculation of Hydration Free Energies using Pair-Specific Lennard-Jones Parameters in the CHARMM Drude Polarizable Force Field. *Journal of Chemical Theory and Computation* **2010**, *6*, 1181–1198.

(69) Fyta, M.; Netz, R. R. Ionic force field optimization based on single-ion and ion-pair solvation properties: Going beyond standard mixing rules. *The Journal of Chemical Physics* **2012**, *136*, 124103(01)–124103(11).

(70) Mamatkulov, S.; Fyta, M.; Netz, R. R. Force fields for divalent cations based on single-ion and ion-pair properties. *The Journal of Chemical Physics* **2013**, *138*, 024505(1)–024505(12).

(71) Yoo, J.; Aksimentiev, A. Improved Parametrization of Li+, Na+, K+, and Mg2+ Ions for All-Atom Molecular Dynamics Simulations of Nucleic Acid Systems. *The Journal of Physical Chemistry Letters* **2012**, *3*, 45–50.

(72) Savelyev, A.; MacKerell, A. D. Balancing the Interactions of Ions, Water, and DNA in the Drude Polarizable Force Field. *The Journal of Physical Chemistry B* **2014**, *118*, 6742–6757.

(73) Li, H.; Ngo, V.; Da Silva, M. C.; Salahub, D. R.; Callahan, K.; Roux, B.; Noskov, S. Y. Representation of Ion–Protein Interactions Using the Drude Polarizable Force-Field. *The Journal of Physical Chemistry B* **2015**, *119*, 9401–9416.

(74) Savelyev, A.; MacKerell, A. D. Competition among Li+, Na+, K+, and Rb+ Monovalent Ions for DNA in Molecular Dynamics Simulations Using the Additive CHARMM36 and Drude Polarizable Force Fields. *The Journal of Physical Chemistry B* **2015**, *119*, 4428–4440.

(75) Nitta, N.; Wu, F.; Lee, J. T.; Yushin, G. Li-ion battery materials: present and future. *Materials Today* **2015**, *18*, 252 – 264.